Review article
DOI: /10.5513/JCEA01/27.1.5013
Journal of Central European Agriculture, 2026, 27(1), p.261-288

Fingerprinting of soil organic matter composition by attenuated total reflectance – Fourier transform infrared spectroscopy

Karakterizacija organske tvari tla upotrebom prigušene totalne refleksije – infracrvene spektroskopije s Fourierovom transformacijom

Sofia KAPENI[1], Željka ZGORELEC[2] (✉), Ivana ŠESTAK[2], Apolka UJJ[3], Lidija SVEČNJAK[2]

[1] University of Zagreb Faculty of Agriculture, Svetošimunska cesta 25, Zagreb, Croatia, student Danube AgriFood Joint ERASMUS+ Master (DAFM-Sustainability in Agriculture, Food Production and Food Technology in the Danube Region)

[2] University of Zagreb Faculty of Agriculture, Svetošimunska cesta 25, Zagreb, Croatia

[3] Hungarian University of Agriculture and of Life Sciences, Institute of Rural Development and Sustainable Economy, Agroecology and Ecological Farming Department, Gödöllő, Hungary

✉ Corresponding author: zzgorelec@agr.hr

Received: September 18, 2025; accepted: January 22, 2026

ABSTRACT

Fourier transform infrared spectroscopy (FTIR), as a non-destructive method, is a powerful tool that provides insights into SOM functional groups and other soil dynamic properties. This study aims to provide a comprehensive review of the use of FTIR spectroscopy for the spectral characterization of soil constituents, both organic and inorganic, along with a case study evaluating the applicability of Attenuated Total Reflectance - Fourier Transform Infrared Spectroscopy (ATR-FTIR) for SOM characterisation in five Croatian soil types. The investigated soil types were: Luvisol, Regosol acric, Gleysol vertic, Dystric Stagnosol and Chernozem, which differ in various soil indicators, including organic matter content (OM), pH, clay content, total nitrogen (TN), plant available phosphorus (P_{AL}) and potassium (K_{AL}). According to our findings, ATR-FTIR spectroscopy provided insights into the inorganic and organic soil constituents. The FTIR spectra indicated that only the hydrophilic fraction of the SOM of all five soil types analyzed was detected. However, strong absorbance bands attributed to minerals and other inorganic constituents of soils masked (overlapped) the molecular vibrations of distinct SOM constituents, highlighting the need for further sample pretreatment and advanced chemometric modelling techniques to fingerprint SOM composition using ATR-FTIR spectroscopy.

Keywords: ATR-FTIR spectroscopy, case study, Croatian soil types, FTIR chemical characterization, soil organic matter, soil properties

SAŽETAK

Infracrvena spektroskopija s Fourierovom transformacijom (FTIR), kao ne destruktivna metoda, predstavlja snažan alat koji pruža uvid u funkcionalne skupine organske tvari tla (OT) i druga dinamička svojstva tla. Cilj ovog rada je pružiti sveobuhvatan pregled primjene FTIR spektroskopije za spektralnu karakterizaciju sastavnica OT tla, kako organskih tako i anorganskih, uz studiju slučaja o utvrđivanju primjenjivosti i učinkovitosti infracrvene spektroskopije s Fourierovom transformacijom i primjenu prigušene totalne refleksije (ATR-FTIR) za karakterizaciju OT u pet različitih tipova tla. Istraživani tipovi tla bili su: Luvisol (crvenica/terra rossa), Regosol acric (regosol na eolskom pijesku), Gleysol vertic (glejno vertično), Dystric Stagnosol (pseudoglej) i Chernozem (černozem/crnica), koji se razlikuju prema specifičnim deskriptorima tla, kao što su sadržaj organske tvari (OT), pH vrijednost, udio gline, sadržaju ukupnog dušika (TN), biljkama pristupačnog fosfora (P_{AL}) i kalija (K_{AL}). Prema našim rezultatima, ATR-FTIR spektroskopija omogućila je uvid u

anorganske i organske sastavnice tla. FTIR spektri pokazali su da je detektirana samo hidrofilna frakcija OT kod svih pet analiziranih tipova tla. Međutim, snažne apsorpcijske vrpce pripisane mineralima i drugim anorganskim sastavnicama tla maskirale su (preklapale) molekulske vibracije pojedinih sastavnica OT, što naglašava potrebu za dodatnom pred pripremom uzoraka i primjenu naprednih kemometrijskih metoda modeliranja za određivanje „otiska prsta" sastava OT primjenom ATR-FTIR spektroskopije.

Ključne riječi: ATR-FTIR spektroskopija, studija slučaja, tipovi tla u RH, FTIR kemijska karakterizacija, organska tvar tla, svojstva tla

INTRODUCTION

Soil organic matter (SOM) has a profound effect on the soil's physical, chemical and biological properties (Cooperband, 2002; Lehman et al., 2015; Baumann et al., 2016; Wang et al., 2023; Thabit et al., 2024). SOM derives from plant and animal residues in different degrees of degradation and plays a vital role in microbial decomposition processes, particularly humification (Cooperband, 2002; Bot and Benites, 2005; Haynes, 2005; Xing et al., 2021). This heterogeneity in the composition of SOM, along with the adsorption of metal oxides, such as aluminum (Al) and iron (Fe) hydrous oxides, can affect SOM humification. More specifically, the negatively charged humic molecules of SOM create strong bonds with the surfaces of Al and Fe, thus resulting in the formation of macroaggregates (Cooperband, 2002; Haynes, 2005; Wasner et al., 2024). The bonding and binding agents of SOM are crucial for the formation of organo-mineral complexes as well as the stabilization of SOM (Cooperband, 2002; Lal et al., 2015; Lehman et al., 2015; Dhillon et al., 2017; Jiménez-González et al., 2019).

Over the past three decades, spectroscopy has emerged as a cost- and time-effective tool for assessing soil properties, simultaneously (Nocita et al., 2015; Rial et al., 2016; Seybold et al., 2019; Allo et al., 2020; Metzger et al., 2020; Sanderman et al., 2020; Nath et al., 2022; Lei et al., 2023; Ye et al., 2024). Due to the minimal labor, simple sample preparation, and the small quantity of soil samples required, soil spectroscopy enables more precise analysis compared to traditional techniques (Stenberg et al., 2010; Xing et al., 2021). Moreover, spectroscopy has proven advantageous in studying interactions between organic and mineral constituents within soil, whereas conventional laboratory methods are less effective in providing insights into these interactions (Volkov et al., 2021). Infrared spectroscopy (IR) has been primarily used in assessing SOM, soil organic carbon (SOC) humic substances (aliphatics, aromatics), minerals (clay, silt, sand, carbonates), potassium (K), phosphorus (P), magnesium (Mg), calcium (Ca), lattice water, pH, and cation exchange capacity (CEC) (Zimmermann et al., 2007; Demyan et al., 2012; Bruckman et al., 2013; Soriano-Disla et al., 2013; Hutengs et al., 2019; Allo et al., 2020; Jensen et al., 2020; Helfenstein et al., 2021; Huang et al., 2024). The abovementioned soil compounds are recognized as spectrally active compounds that can develop fundamental absorptions in the infrared region (Vohland et al., 2014; Seybold et al., 2019; Metzger et al., 2020; Wijewardane et al., 2021).

Fourier Transform Infrared Spectroscopy (FTIR) serves as a powerful tool for analyzing soil without the need for chemical extraction, thereby avoiding interference from secondary chemical reactions and artefacts associated with extraction processes (Maynard and Johnson, 2018; Pärnpuu et al., 2022; Nath et al., 2022; Margenot et al., 2023). FTIR effectiveness lies in the capability to detect functional groups that change dipole moments and can absorb infrared radiation. These functional groups contain oxygen (O), nitrogen (N), and sulfur (S) atoms, exhibiting high chemical reactivity, such as cation-exchange capacity and metal sorption (Margenot et al., 2017).

This research is based on the hypothesis that FTIR spectroscopy can be used to assess SOM. This study aimed to provide a comprehensive review of soil spectroscopy, along with a case study on evaluating the applicability of Attenuated Total Reflectance - Fourier Transform Infrared Spectroscopy (ATR-FTIR) for SOM analysis

in five Croatian soil types. The examined soil types were: Luvisol, Regosol acric, Gleysol vertic, Dystric Stagnosol and Chernozem, which exhibit variations in various soil indicators including organic matter content (OM), pH, total nitrogen (TN), plant available phosphorus (P_{AL}) and potassium (K_{AL}), and clay content.

Therefore, the objectives of this study were (i) to provide an extensive review of the scientific literature on the utilization of FTIR spectroscopy for chemical characterization and spectral analysis of SOM in the MIR spectral range; (ii) to evaluate the effectiveness of ATR-FTIR spectroscopy in characterizing SOM based on a case study covering five distinctive soil types sampled in Croatia; and (iii) to perform a comparative overview of FTIR chemical fingerprints of five distinctive soil types.

FTIR spectroscopy and soil analysis

Numerous studies have identified characteristic molecular vibrations corresponding to soil organic and inorganic constituents within the FTIR spectra. The study of Volkov et al. (2021) emphasized the importance of ATR-FTIR in achieving enhanced sensitivity in the determination of SOM and SOC. A recent study of Jackson Soil and Root Ecology Lab (2023) investigated the degradation of SOM using FTIR spectroscopy. Lei et al. (2023) and Jadhav et al. (2024) explored the effect of SOM chemical composition on its stabilization processes. Margenot et al. (2017) suggested in their study that the presence of absorbance bands that correspond to aliphatic and aromatic compounds within the soil spectrum indicates the level of humification, and thus SOM characterization. The humification index of SOM was also investigated in the study of Obeng et al. (2023). In addition, FTIR has been successfully used to evaluate the hydrophobicity, based on the soil's content in aliphatic substances (Margenot et al., 2017; Pärnpuu et al., 2022). Notably, Ye et al. (2024) demonstrated that hydrofluoric acid pretreatment can enhance the ability of FTIR to detect carbohydrate and aliphatic C–H bands in specific spectral regions within the MIR range.

Furthermore, Parolo et al. (2017) highlighted the critical role of hydrophilic and hydrophobic constituents in shaping the spatial and structural configurations of carbon chains within SOM. More specifically, the hydrophilic and hydrophobic constituents of SOM can develop hydrogen bonds and cation exchanges with clay minerals, thus influencing SOM's chemical properties. Helfenstein et al. (2021) focused their study on the efficacy of MIR spectroscopy in predicting soil carbon and demonstrated that, when combined with appropriate statistical models, it can enhance the accuracy of assessing soil properties and can be used to develop soil spectral libraries for different soil types. Along with the studies mentioned above, a comprehensive set of other research has reported results from spectral analysis of soil in the MIR region, covering various aspects of soil characterization.

Spectral analysis of soil in the MIR region

A summary of the IR signals and associated functional group vibrations reported in the available scientific literature is presented in Table 1, comprising assignation of nearly 300 absorption bands reported for soil. According to the study of Tinti et al. (2015) and the references therein, Si–OH and Fe–O stretching vibrations at 3698 cm^{-1} and 3622 cm^{-1} are indicative of phyllosilicates within the clay minerals of kaolinite and gibbsite. Similar findings of silicates are also observed in several other studies, such as O–H stretching between 3696 cm^{-1} and 3617 cm^{-1} (Padilla et al., 2014; Parolo et al., 2017; Ghebleh-Goydaragh et al., 2021a; Volkov et al., 2021; Xing et al., 2021; Pärnpuu et al., 2022), as well as (Al)/(Mg) Si–OH stretching at 3620 – 3613 cm^{-1} assigned to the clay minerals of kaolinite, montmorillonite and smectite (Peltre et al., 2014; Fakhry et al., 2016; Xu et al., 2020; Volkov et al., 2021; Krivoshein et al., 2022). Moreover, Fe–O stretching of silicates within kaolinite and gibbsite is observed at 3622 cm^{-1} (Tinti et al., 2015). Various studies also highlighted the overlapping signals of inorganic and organic compounds in the region 3600 – 3360 cm^{-1}, mainly characterized by the prevalence of O–H and N–H stretching vibrations, attributed to clay minerals, such

as gibbsite, along with carboxyl and hydroxyl groups of SOM, such as amines, amides, alcohols, phenols, and carboxylic acids (Tinti et al., 2015; Dhillon et al., 2017; Parolo et al., 2017; Nuzzo et al., 2020; Xu et al., 2020; Ghebleh-Goydaragh et al., 2021b; Volkov et al., 2021; Xing et al., 2021; Krivoshein et al., 2022; Pärnpuu et al., 2022). Additionally, Artz et al. (2008) reported the presence of cellulose at 3340 cm^{-1}. These findings emphasize the complex interaction between clay minerals and organic compounds within the soil. Organic compounds are also present in the region 3270 – 3042 cm^{-1}, including aromatic phenols and alcohols (Artz et al., 2008; Teong et al., 2016; Volkov et al., 2021).

The prevalence of C–H stretching vibrations has been extensively reported in the region 3000 – 2800 cm^{-1}, attributed to aliphatic compounds, such as lipids. These compounds constitute the hydrophobic fraction of SOM, as confirmed by numerous reports (Padilla et al., 2014; Peltre et al., 2014; Baumann et al., 2016; Fakhry et al., 2016; Dhillon et al., 2017; Maynard and Johnson, 2018; Nuzzo et al., 2020; Ghebleh-Goydaragh et al., 2021a; Helfenstein et al., 2021; Volkov et al., 2021; Krivoshein et al., 2022; Pärnpuu et al., 2022; Obeng et al., 2023). In addition, Obeng et al. (2023) reported the presence of humic acids, fulvic acids and humin in the spectral range between 2856 and 2849 cm^{-1}. Besides, C–H stretching vibrations around 2850 cm^{-1} are assigned to aliphatics and polysaccharides (Artz et al., 2008; Teong et al., 2016; Nuzzo et al., 2020).

The presence of carbonates within soil spectra has been confirmed by several studies. The C–H vibrations in the 2627 – 2400 cm^{-1} range (Peltre et al., 2014; Tinti et al., 2015; Parolo et al., 2017; Helfenstein et al., 2021; Ghebleh-Goydaragh et al., 2021a) and 1800 – 1783 cm^{-1} (Tinti et al., 2015; Volkov et al., 2021) are attributed to carbonate minerals, such as aragonite, calcite and dolomite. Nevertheless, Krivoshein et al. (2022) reported the presence of clay minerals and quartz between 1880 and 1866 and at 1783 cm^{-1}, while Fakhry et al. (2016) indicated the presence of humic acids between 1900 and 1700 cm^{-1}.

The hydrophilic fraction of SOM is extensively observed in soil spectra within the MIR range. Particularly, the spectral range between 1730 and 1700 cm^{-1} is characterized by the prevalence of C=O stretching vibrations of carboxylic acids (Teong et al., 2016; Dhillon et al., 2017; Nuzzo et al., 2020; Ghebleh-Goydaragh et al., 2021b; Volkov et al., 2021; Obeng et al., 2023). A series of absorption bands related to SOM constituents, like C=C and C=O, C=N stretching vibrations and N–H, C–N bending vibrations, are observed in the 1670 – 1444 cm^{-1} range, indicative of aromatics (Volkov et al., 2021; Krivoshein et al., 2022; Pärnpuu et al., 2022), aliphatics (Peltre et al., 2014; Ghebleh-Goydaragh et al., 2021b; Helfenstein et al., 2021), phenolics (Dhillon et al., 2017; Parolo et al., 2017; Jiménez-González et al., 2019), amide I and II (Padilla et al., 2014; Teong et al., 2016; Parolo et al., 2017; Xu et al., 2020; Helfenstein et al., 2021; Krivoshein et al., 2022), ketones (Dhillon et al., 2017; Maynard and Johnson, 2018), quinones (Jiménez-González et al., 2019; Obeng et al., 2023), lignin (Artz et al., 2008; Dhillon et al., 2017; Ghebleh-Goydaragh et al., 2021b).

The range between 1465 and 1410 cm^{-1} is dominated by C–H and N–H stretching vibrations, attributed to organic compounds, such as amides, aliphatics, aromatics, and phenolics, as well as C–H stretching vibrations of carbonates and clay minerals (Tinti et al., 2015; Baumann et al., 2016; Helfenstein et al., 2021; Volkov et al., 2021; Xing et al., 2021; Pärnpuu et al., 2022; Krivoshein et al., 2022). Organo-mineral complexes observed at 1465 – 1460 cm^{-1} appear due to SiO–H vibrations of silicates along with C–O–H and C–H vibrations of aliphatics (Peltre et al., 2014; Volkov et al., 2021; Krivoshein et al., 2022). Moreover, various studies have reported C–O stretching vibrations attributed to both inorganic and organic compounds within the 1453 – 1410 cm^{-1} spectral range. These vibrations are associated with carbonate minerals such as calcite and dolomite, and organic compounds such as aromatics, aliphatics, phenolics (Peltre et al., 2014; Tinti et al., 2015; Fakhry et al., 2016; Dhillon et al., 2017; Ghebleh-Goydaragh et al., 2021b; Helfenstein et al., 2021; Volkov et al., 2021; Xing et al., 2021; Obeng et al., 2023). Furthermore, Artz et al. (2008) reported

C–O, C=C, and O–H stretching vibrations as indicative of humic acids and carboxylic acids at 1426 cm^{-1}, while Volkov et al. (2021) observed at 1420 cm^{-1} (Mg)–OH and C–O vibrations associated with clay minerals and carboxylic acids, respectively.

The study of Ghebleh-Goydaragh et al. (2021a) revealed O–H stretching vibrations of clay minerals, such as montmorillonite and nontronite, in the spectral region between 1400 and 1300 cm^{-1}, while in the 1396 – 1383 cm^{-1} range, Parolo et al. (2017) reported C–O stretching vibrations of both carbonates (calcite, dolomite) and organic compounds (aromatics, phenolics). In addition, Dhillon et al. (2017) assigned C–O vibrations observed at 1370 cm^{-1} to lignin-derived phenols and aliphatics. The C–N stretching vibrations observed in the 1342 – 1307 cm^{-1} range are indicative of aromatic amines, as stated by Tinti et al. (2015). In the range of 1320 – 1310 cm^{-1}, Volkov et al. (2021) reported the presence of C–H and C–O stretching vibrations and assigned them to amides (amide III), aromatics and carboxylic acids, while Helfenstein et al. (2021) observed O–H deformations of carbonates. Additionally, Padilla et al. (2014) reported C–H, C–O, O–H deformations of amide II, carboxylic acids, phenols and ester in the 1320 – 1220 cm^{-1} spectral range.

According to Tinti et al. (2015), the C–O stretching vibrations in the range 1293 – 1256 cm^{-1} are indicative of bentonite and benzoic acid. Krivoshein et al. (2022) also reported C–O stretching vibrations at 1285 – 1280 cm^{-1} attributed to clay minerals as well as aromatics and carboxylic acids. Further C–O stretching vibrations of phenolics are also observed at 1295 – 1220 cm^{-1} by Peltre et al. (2014), at 1265 cm^{-1} by Artz et al. (2008) and at 1240 cm^{-1} by Maynard and Johnson (2018). Many studies have revealed the presence of several other organic and inorganic compounds in the range 1285 – 1110 cm^{-1}, including silicates of clay minerals and quartz, aromatics, phenolics, aliphatics, cellulose, carbohydrates, alkyl ethers and esters (Artz et al., 2008; Tinti et al., 2015; Dhillon et al., 2017; Nuzzo et al., 2020; Volkov et al., 2021; Krivoshein et al., 2022; Obeng et al., 2023). Lignin structures are observed at 1270 cm^{-1}, 1230 cm^{-1}, and 1130 cm^{-1} according to Jiménez-González et al. (2019), and at 1265 cm^{-1} according to Artz et al. (2008). It is also noteworthy that Dhillon et al. (2017) reported C–O vibrations at 1160 – 1030 cm^{-1} assigned to cellulose, and Padilla et al. (2014) denoted C–O vibrations to carbohydrates, proteins and nucleic acids at 1170 – 1000 cm^{-1}.

The region between 1107 and 910 cm^{-1} is a complex and the most intensive segment of soil ATR-FTIR spectrum dominated by a wide range of vibrations including (Al)–OH, Si–O, C–OH, C–O, C–N deformations attributed to silicates, aromatic (benzoic acid, lignin) and non-aromatic (polysaccharides, carbohydrates, cellulose) compounds (Tinti et al., 2015; Baumann et al., 2016; Parolo et al., 2017; Nuzzo et al., 2020; Xu et al., 2020; Volkov et al., 2021; Xing et al., 2021; Krivoshein et al., 2022; Pärnpuu et al., 2022; Obeng et al., 2023). Particularly, (Al)–OH stretching of aluminosilicates has been extensively reported at 926 – 910 cm^{-1}. Mentioned silicates are primarily related to clay minerals such as kaolinite, illite, smectite, montmorillonite and nontronite (Tinti et al., 2015; Fakhry et al., 2016; Dhillon et al., 2017; Xu et al., 2020; Volkov et al., 2021; Ghebleh-Goydaragh et al., 2021a; Xing et al., 2021; Krivoshein et al., 2022). The absorption bands of Si–OH, (Al)/(Mg)/(Fe)–OH, which are prevalent in the spectral range between 891 and 700 cm^{-1}, unveil the dominance of inorganic soil constituents, including carbonates, such as calcite, clay minerals and quartz (Artz et al., 2008; Nuzzo et al., 2020; Xu et al., 2020; Ghebleh-Goydaragh et al., 2021a; Volkov et al., 2021; Krivoshein et al., 2022).

The presence of C–H bending vibrations of aromatic compounds at 875 cm^{-1}, 750 cm^{-1}, 715 cm^{-1} and 675 – 670 cm^{-1} is reported by Volkov et al. (2021), and at 698 – 686 cm^{-1} by Parolo et al. (2017). Furthermore, N–H bending vibrations of primary and secondary amines are evident in the studies of Peltre et al. (2014) at 850 – 700 cm^{-1} and Xu et al. (2020) at 780 cm^{-1}. Metal oxides, mainly Fe oxides, were reported by Peltre et al. (2014) at 700 – 600 cm^{-1}, and by Fakhry et al. (2016) at 794 – 777 cm^{-1} and at 536 – 525 cm^{-1}. Lastly, Si–O bending vibrations below 535 cm^{-1} are attributed to quartz and clay minerals such

as kaolinite, illite, and smectite (Tinti et al., 2015; Nuzzo et al., 2020; Volkov et al., 2021; Krivoshein et al., 2022). All of the abovementioned IR absorption band positions along with the assignment of the underlying molecular vibrations (assigned functional groups) and associated soil constituents, are summarized in Table 1.

MATERIALS AND METHODS

Case study

Soil properties

Croatia is characterized by diverse topographic configurations contributing to a wide variety of soil types. Five soil samples were collected from the topsoil of various locations across Croatia (Figure 1).

The collected soil types originated from regions with varying pedogenic characteristics and land use practices. The classification of these soil types was carried out in accordance with the World Reference Base for Soil Resources (WRB) (FAO, 2015) and the national classification system for the soils of Croatia, established by Bašić (2013). The sampling parameters of the studied soils, including soil type, geographical coordinates, sample location and region, type of land use, sampling depth, and year of sampling, are summarized in Table 2.

In western Croatia, in the region of Novigrad in the Peninsula of Istria, the selected soil type was Luvisol. The soil sample was obtained from an area combining olive tree cultivation with fire range (Figure 2a). Luvisol, which is also known as “terra rossa”, is the most widely distributed soil across Croatia (Bašić, 2013).

Figure 1. Spatial distribution of soil sampling sites across Croatia (West: Novigrad, Central: Potok, North: Molve, East: Vukovar)

The parent material of Luvisols may vary from non-calcareous to limestone substrates. Limestone substrates typically have a higher concentration of clay minerals compared to silicate substrates. Luvisols are characterized by the accumulation of inorganic and organic materials in the upper horizons, resulting in the formation of a surface layer enriched with organic matter. Within Luvisols, humification leads to the formation of organic compounds with low molecular weight that can easily bind with aluminum and iron ions under acidic conditions. Consequently, mineral leaching occurs, thus reducing the stability of clay minerals like montmorillonite (Bašić, 2013).

In northern Croatia, within the region of Molve, the two soil types selected were the Regosol acric (Figure 2b) and Gleysol vertic (Figure 2c). Regosol acric was obtained from an arable land in Molve 40, and Gleysol vertic was obtained from meadow land in Molve 9. Regosols are undeveloped soils primarily formed by erosion processes, particularly water erosion, that gradually remove soil materials (Bašić, 2013). Gleysols are characterized by heavy texture and high clay content, particularly montmorillonite. Chemically, Gleysols are distinguished by their high organic matter content, ranging from 1.4% to 9.1%, high cation exchange capacity (CEC), and absence of acidic properties. As a result, Gleysols are rich in available nutrients; however, under anaerobic conditions, their nutrient availability and, thus, the soil dynamics are affected (Bašić, 2013).

In the northeastern part of Croatia, in the region of Potok, the soil type of Dystric Stagnosol was collected from an arable cropland (Figure 2d). Notably, Stagnosols are the second most widely distributed soil across Croatia, after Luvisol. Stagnosol, also known as Pseudogley, is distinguished by waterlogging conditions caused by excessive rainwater, leading to gleyization processes. Stagnosols are typically formed from leached loess or fluviatile/colluvial sediments in non-calcareous clay minerals and are characterized by high silt content due to eolian sedimentations (Bašić, 2013).

a) Luvisol

b) Regosol acric

c) Gleysol vertic

d) Dystric Stagnosol

e) Chernozem

Figure 2. Soil type

Within Vukovar in Eastern Croatia, which is a region extensively known for its conventional agricultural use, the sampled soil was Chernozem (Figure 2e). Chernozems are characterized by a loamy texture, which is predominantly composed of illite clay minerals, and are known for accumulating high-quality organic matter. Chernozems are naturally rich in nutrients, especially in phosphorus and potassium. However, due to anthropogenic interventions and intensive agricultural practices, they may experience a decline in organic matter content and the overall soil fertility (Bašić, 2013).

Reference physicochemical analyses

The physicochemical properties of the soils were first analyzed by using standardized methods. Soil sample preparation involved drying, grinding, sieving and homogenizing of soil samples according to the standard ISO 11464:2006. The particle size distribution was defined by sieving and sedimentation (ISO 11277:2009). The pH was measured in three different solutions: 0.01 M $CaCl_2$, 1 M KCl, and H_2O, modified at a 1:2.5 w/v ratio, according to the standard ISO 10390:2005. The organic matter (OM) content was determined as a percentage of dry matter (% DM) using the sulfochromic oxidation method (modified Tjurin method) in accordance with ISO 14235:2004. Total nitrogen (TN) content was determined as a percentage of dry matter (% DM) using dry combustion method ("elemental analysis"), following the standard ISO 13878:2004. The availability of phosphorus (P) and potassium (K) was determined by the ammonium lactate (AL) method with an extraction using ammonium lactate and acetic acid at a 1:20 w/v ratio (Škorić, 1982).

ATR-FTIR analysis and IR spectra acquisition

The air-dried soil samples were analyzed by Attenuated Total Reflectance - Fourier Transform Infrared Spectroscopy (ATR-FTIR) recording technique. ATR-FTIR spectra of the soil samples were acquired using the Cary 660 FTIR spectrometer (Agilent Technologies) coupled with a Golden Gate single-reflection diamond ATR accessory (Specac). Absorbance spectra were recorded in the mid-infrared region (4000 – 400 cm^{-1}) at a nominal recording resolution of 4 cm^{-1}. Before the spectral analysis, samples were pulverized into fine homogenates with a mortar. For spectra acquisition, approximately 10 mg of the homogenized soil sample was pressed on the diamond ATR plate using a self-levelling sapphire anvil to obtain the ATR-FTIR spectrum of a thin, uniform layer of each sample. Spectra were recorded in absorbance mode, and 32 scans/spectrum were acquired. Four replicate spectra of each sample were acquired by using different aliquots, and the average of those was calculated. The ATR element was thoroughly cleaned with distilled water and dried with soft tissue paper prior to each spectrum acquisition. A background spectrum was recorded between each sample acquisition. The laboratory temperature was maintained at 23 ± 1 °C during the measurements. The assignation of the molecular vibrations of the soil spectra was conducted based on the spectral atlas of Socrates's tables and charts of IR spectra and characteristic group frequencies (Socrates, 2001), and spectral data from the scientific literature.

Statistical analysis

The raw spectral data were stored and pre-analyzed using the Resolutions Pro version 5.3.0 software package. Further spectral data analysis and processing were carried out using Origin 8.1 (OriginLab Corporation).

RESULTS AND DISCUSSION

Physicochemical properties

The results of the physical and chemical analysis performed on the soil samples are shown in Tables 3 and 4, respectively. The organic matter (OM%) varied from 1.3% in Dystric Stagnosol (weakly humic soil) to 10.9% in Gleysol vertic (highly humic soil) (Škorić, 1982; Šoštarić et al., 2017; Zebec et al., 2017). Notably, Gleysol vertic, characterized by 54% clay content (clay texture), had the highest OM% content among the soils. Conversely, Dystric Stagnosol, with 14.1% clay content (sandy loam texture), had the lowest OM% content. The pH ranged from acidic (4.83) in Gleysol vertic to neutral (6.80) in Chernozem. The total nitrogen content ranged from 0.08% in

Dystric Stagnosol (soil weakly supplied with N), to 0.71% in Gleysol vertic (soil very rich in N). The concentration of available phosphorus (P) ranged from 30 mg/kg in Gleysol vertic (soil very poorly supplied with P), to 315 mg/kg in Chernozem (soil very rich in P). The concentration of available potassium (K) ranged from 129 mg/kg in Dystric Stagnosol (soil moderately supplied in K) to 431 mg/kg in Chernozem (soil very rich in K) (Zebec et al., 2017).

ATR-FTIR spectral analysis

Assignation of molecular vibrations in soil spectra

The FTIR-ATR spectra of the different soil types (obtained as an average spectrum for each soil sample) with the assignation of the major underlying molecular vibrations are presented in Figure 3. A weak shoulder band was observed at 3646 cm^{-1} in the spectrum of Luvisol. The broad weak peak arising at 3415 cm^{-1} (3500 – 3000 cm^{-1}) is assigned to O–H, Fe–O of clay minerals as well as O–H and N–H stretching vibrations of SOM constituents (Tinti et al., 2015; Fakhry et al., 2016; Parolo et al., 2017; Xu et al., 2020; Ghebleh-Goydaragh et al., 2021b). No IR absorption signals were observed in the spectral region from 3000 to 1800 cm^{-1} of the analyzed soil spectra. The weak peak at 1635 cm^{-1} is assigned to C=C stretching and N–H bending vibrations of amide I, and C=C, C=O stretching vibrations of aromatic compounds such as ketones, aldehydes, quinones, and carboxylic acids (benzoic acid) (Peltre et al., 2014; Tinti et al., 2015; Baumann et al., 2016; Dhillon et al., 2017; Parolo et al., 2017; Jiménez-González et al., 2019; Volkov et al., 2021; Xing et al., 2021; Krivoshein et al., 2022; Pärnpuu et al., 2022; Obeng et al. 2023).

The spectral region between 1400 cm^{-1} and 500 cm^{-1} (the most distinctive segment of the fingerprint region) is populated by a number of absorption bands (Figure 4). The most prominent spectral feature in the fingerprint region is the absorption bands occurring at 994 cm^{-1} and 523 cm^{-1} due to the Si–O stretching vibrations of silicates. The shoulder band at 1164 cm^{-1} is assigned to Si–O stretching vibrations of quartz, and C–O stretching vibrations of aliphatics, alcohols, and polysaccharides (Tinti et al., 2015; Dhillon et al., 2017; Volkov et al., 2021; Krivoshein et al., 2022). The shoulder bands peaking at 1114 cm^{-1} and 1024 cm^{-1} are ascribed to SiO–H vibrations of aluminosilicates within clay minerals, and C–OH, C–O and C–H vibrations of SOM constituents (Peltre et al., 2014; Volkov et al., 2021; Krivoshein et al., 2022; Obeng et al., 2023). Notably, the band at 1114 cm^{-1} was only observed in the spectrum of Luvisol. Therefore, it can be identified as Luvisol-specific, indicating the presence of both aluminosilicates and SOM constituents, whose vibrations overlap at this wavelength. The intensive band at 994 cm^{-1} was followed by a medium intensity signal occurring at 912 cm^{-1} attributed to (Mg/Al)–OH stretching of aluminosilicates within clay minerals, including kaolinite (Fakhry et al., 2016; Nuzzo et al., 2020; Xu et al., 2020; Xing et al., 2021) and C–O–H out-of-plane bending of carbohydrates, cellulose as well as benzoic acid (Volkov et al., 2021; Krivoshein et al., 2022). The very weak band peaking at 831 cm^{-1} can be attributed to C–H vibrations of aromatics and lignin as reported in previous studies (Artz et al., 2008; Tinti et al., 2015; Volkov et al., 2021; Krivoshein et al., 2022).

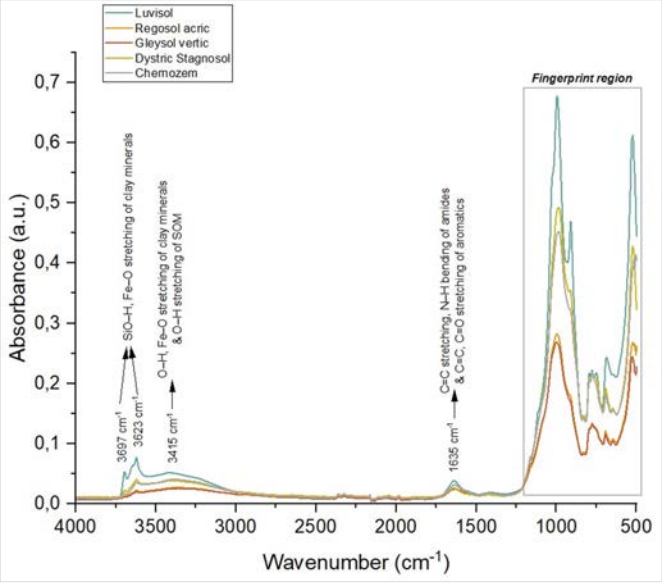

Figure 3. Average ATR-FTIR spectra of different soil types collected across Croatia: comparative spectral features with the assignation of major underlying molecular vibrations (whole spectral region: 4000 to 500 cm^{-1})

The most complex absorption region of the IR spectrum of soil arises below 800 cm^{-1} due to the numerous overlapping bands of inorganic and organic compounds present in soil (Figure 4). The bands of medium intensity peaking at 794 cm^{-1}, 777 cm^{-1}, 748 cm^{-1}, and 692 – 686 cm^{-1} are assigned to Si–O, (Fe/Mg/Al)–OH stretching vibrations of aluminosilicates and quartz, and C–H bending of aromatics and N–H bending of amines (Peltre et al., 2014; Fakhry et al., 2016; Nuzzo et al., 2020; Volkov et al., 2021; Krivoshein et al., 2022; Ye et al., 2024). A very weak band observed at 646 cm^{-1} is attributed to Si–O, S–C, O–H stretching vibrations of silicates, like bentonite, and sulfates (Krivoshein et al., 2022). The most prominent absorption in this region is a broad band with an absorption maximum at 523 cm^{-1} assigned to Si–O bending vibrations of clay minerals (kaolinite) and quartz (Tinti et al., 2015; Volkov et al., 2021).

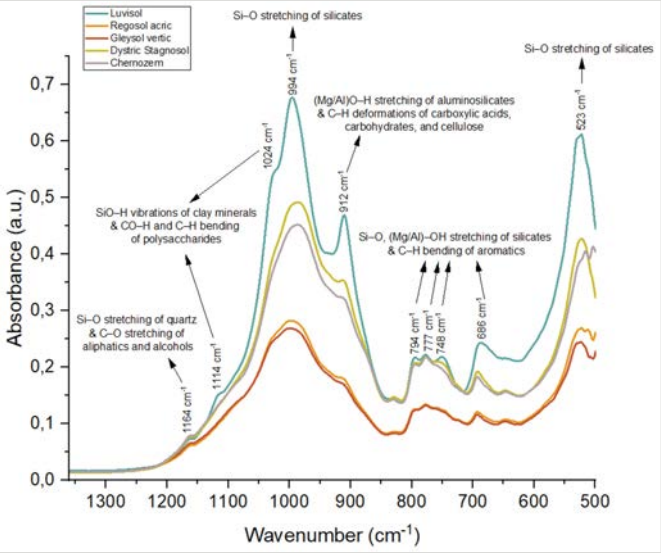

Figure 4. Average ATR-FTIR spectra of different soil types collected across Croatia: comparative spectral features with the assignation of major underlying molecular vibrations (fingerprint region: 1400 to 500 cm^{-1})

Comparison of the characteristic absorption bands between the soil types

Overall, the integral spectral features in terms of band positions appear to be similar among the different soil types. However, variations in absorbance intensities of the observed functional groups were noticeable in the H–bond region (4000 – 3100 cm^{-1}) and the fingerprinting region (1400 – 500 cm^{-1}). The strong absorbance bands observed at 3697 cm^{-1} and 3623 cm^{-1} in all soil types are consistent with the dominance of clay minerals within soil, which is in compliance with findings from several other studies as presented in Table 1. Luvisol had the highest absorbance peaking at 3697 cm^{-1}, 3623 cm^{-1}, 3415 cm^{-1}, while the lowest intensity of absorbance was observed in Gleysol vertic and Regosol acric.

Additionally, the unique weak shoulder band at 3646 cm^{-1} observed in Luvisol, and not in other soil types, suggests a distinctive mineralogical composition of Luvisol. This may be attributed to the high content of Fe oxides, which is evident from its characteristic reddish color (terra rossa). During soil formation, the weathering of minerals influences the concentration of Fe oxides influences the capacity of the soil to adsorb soil organic matter (Rial et al., 2016; Maynard and Johnson, 2018) and, in turn, affects soil color (Baumann et al., 2016; Margenot et al., 2017). The reactive surfaces of Fe-containing minerals provide sites for the formation of organo-mineral complexes (Margenot et al., 2017), creating variations in the color of the soil, depending on the form and concentration of Fe oxides present. Namely, ferrihydrite ($5Fe_2O_39H_2O$) is responsible for giving a reddish-brown color to the soil (Baumann et al., 2016). Therefore, the presence of the band at 3646 cm^{-1}, exclusively observed in Luvisol, can be attributed to Fe oxides bound to minerals. Moreover, the process of organo-mineral complexation plays a critical role in humification and SOM stabilization (Bot and Benites, 2005; Baumann et al., 2016), suggesting that Luvisol may be characterized by a higher content of organo-mineral complexes and, hence, of stable SOM fraction compared to the other soils studied. These complexes, particularly those composed of hydrophilic compounds, are more readily adsorbed onto clay mineral surfaces (Pärnpuu et al., 2022).

The ATR-FTIR spectra of the studied soil types in the range of 3000 – 1800 cm^{-1} did not result in significant absorptions, indicating the absence of functional groups related to the hydrophobic fraction of SOM. This may be due to the fact that hydrophobic substances, such as ali-

phatics, can be degraded more easily by soil microorganisms than the hydrophilic compounds, while hydrophilic compounds are less accessible to soil microorganisms (Pärnpuu et al., 2022).

The range between 2500 and 800 cm^{-1} is mainly indicative of the presence of organic matter constituents within the soil. According to our ATR-FTIR soil spectra, the IR signal at 1635 cm^{-1} is the only significant band that demonstrates the presence of amides and other aromatic compounds, such as ketones, aldehydes, quinones, and carboxylic acids (benzoic acid), related to the hydrophilic part of SOM (Parolo et al., 2017; Pärnpuu et al., 2022). Although we did not observe significant intensity variations of the amide I band occurring at 1635 cm^{-1} between the soil types, Luvisol demonstrated higher absorbance. This suggests that Luvisol had a higher content of clay minerals and amide I within its organic matter, compared to the other soil types examined.

Our findings exhibited overlapping absorptions of minerals with soil organic matter in the fingerprint region between 1400 cm^{-1} and 500 cm^{-1}. In the 1200 – 1000 cm^{-1} range, only weak shoulder bands were observed at 1164 cm^{-1}, 1114 cm^{-1} and 1024 cm^{-1} attributed to silicates and masked SOM constituents. The shoulder band at 1164 cm^{-1} assigned to vibrations of both inorganic (clay minerals and quartz) and organic compounds (aliphatics, alcohols, carbohydrates), exhibited the highest intensity within the spectra of Chernozem, Dystric Stagnosol, and Luvisol, while Gleysol vertic and Regosol acric had lower intensities. It is noteworthy that the weak band at 1114 cm^{-1} was only observed in the spectrum of Luvisol. This indicates a different composition of Luvisol within this range compared to the other soils. In addition, the spectral range between 1050 and 950 cm^{-1} was dominated by strong overlapping absorptions observed in all soil spectra. This overlapping can mask the characteristic bands of SOM, making it difficult to resolve the SOM content within soil spectra, as also noted in the research by Ye et al. (2024). The highest intensity of the shoulder band at 1024 cm^{-1} was recorded in Luvisol, while the lowest was observed in Gleysol vertic and Regosol acric. These findings suggest that Luvisol, Chernozem, and Dystric Stagnosol have a higher concentration of inorganic and organic constituents.

Within the spectral region between 1050 cm^{-1} and 850 cm^{-1} differences between absorbance bands of the soil types were observed, indicating variability related to the particular constituents of the distinctive soil types. The bands at 993 cm^{-1} and 912 cm^{-1} appeared as sharp peaks with the highest intensity in the spectrum of Luvisol, while Gleysol vertic and Regosol acric displayed the lowest intensities. In addition, the very weak band absorbance observed at 831 cm^{-1} had a higher intensity in Chernozem, Dystric Stagnosol and Luvisol, and a lower intensity in Gleysol vertic and Regosol acric. The soil spectra of Luvisol, Chernozem and Dystric Stagnosol within the series of bands at 794 cm^{-1}, 777 cm^{-1} and 748 cm^{-1} resulted in higher intensities compared to Regosol acric and Gleysol vertic. Finally, at the peak of 692–686 cm^{-1} and 523 cm^{-1} Luvisol exhibited the highest intensity, while Gleysol vertic and Regosol acric exhibited the lowest intensities. These spectral variations among the investigated soil types indicate differences in their constituents, thereby revealing distinct chemical compositions.

These qualitative spectral observations highlight the importance of distinguishing the inorganic constituents of the soils, which can affect SOM content and composition. The chemical analysis further supports this, as it indicates that both Luvisol and Chernozem are characterized by a high content of total N, plant-available P and K. Interestingly, Gleysol vertic although characterized by high clay content (54%) and an extremely high soil organic matter content (10.9 %) (Table 4), as obtained by the conventional analysis, did not reflect such a high SOM content within the ATR-FTIR spectrum. This suggests that FTIR spectra might not distinctly reflect the high SOM content due to the dominance of minerals and related overlapping spectral effects. Given the complexity of soil composition and the overlapping spectral features, it is likely that the high SOM content in Gleysol vertic soil is primarily due to the formation of organo-mineral complexes in the soil (Bot and Benites, 2005).

Consequently, these findings highlight the complexity of soil composition and the challenge of fingerprinting SOM. Therefore, spectral pretreatments (preprocessing of spectral data) coupled with chemometric modelling are highly recommended in order to elucidate overlapping spectral effects, enhance targeted signals and/or suppress unwanted spectral features, depending on the aim of the study.

CONCLUSION

This research aimed to investigate the applicability of ATR-FTIR spectroscopy for soil organic matter characterization. Overall, the ATR-FTIR spectra of five distinct soil types collected from Croatia displayed similar integral spectral features within the MIR range. However, detailed analysis revealed indicative spectral differences between the investigated soil samples. The spectra of Luvisol and Chernozem showed higher absorbances throughout the MIR range, while Regosol acric and Gleysol vertic showed lower absorbances. Notably, Luvisol's characteristic red color ("terra rosa") is attributed to a higher content of Fe oxides.

According to our findings in terms of both an overview of spectral features of soil based on literature data and the results of the presented case study, ATR-FTIR spectroscopy has been demonstrated to be only partially successful in fingerprinting SOM. The obtained FTIR spectra revealed the prevalence of inorganic functional groups throughout the MIR range and only one peak indicative of the hydrophilic fraction of SOM exclusively. However, it can be assumed that other absorption bands assigned to SOM are overlapped with the stronger IR signals of inorganic soil compounds within the MIR range. This extensive overlapping confirms that soil composition is influenced by several factors, making it challenging to fingerprint SOM.

It should be emphasized that FTIR spectroscopy enables the rapid and cost-effective analysis of a large number of soil samples, making it a valuable tool for SOM characterization. Further improvement could be achieved by including a quantitative assessment of FTIR analysis, based on a larger number of samples. Combined qualitative and quantitative analysis of soils, including preprocessing of spectral data (e.g. normalization, multiplicative signal correction - MSC, standard normal variate - SNV, Savitzky-Golay filtering, Norris-Williams derivatives, deconvolution) and chemometric modeling would be beneficial for fingerprinting SOM using FTIR spectroscopy.

Overall, FTIR represents a powerful screening tool; however, quantitative SOM analysis requires the support of a larger number of samples and chemometric calibration models. Advanced multivariate statistical analyses, such as principal component regression (PCR), hierarchical cluster analysis (HCA), linear discriminant analysis (LDA) and/or partial least squares regression (PLSR), which enable the investigation of larger sets of soil samples, could enhance the interpretation of spectral data and enable better elucidation of the relationships between spectral and physicochemical properties of soil. As evidenced by the Gleysol vertic sample, where high organic matter content was not clearly reflected in the FTIR spectrum due to the dominance of minerals, sample pretreatment methods such as incineration or ashing are essential for enabling more accurate characterization of SOM composition. Altogether, these approaches are essential not only for enhancing the applicability of FTIR analysis in fingerprinting SOM but also for advancing the overall soil quality assessment.

REFERENCES

Allo, M., Todoroff, P., Jameux, M., Sterna, M., Paulina, L., Albrecht, A. (2020) Prediction of tropical volcanic soil organic carbon stocks by visible-near- and mid-infrared spectroscopy. Catena, 189, 104452. DOI: https://doi.org/10.1016/j.catena.2020.104452

Artz, R. R. E., Chapman, S. J., Robertson, A. H. J., Potts, J. M., Laggoun-Défarge, F., Gogo, S., Comont, L., Disnar, J.-R., Francez, A.-J. (2008) FTIR spectroscopy can predict organic matter quality in regenerating cutover peatlands. Soil Biology and Biochemistry, 40 (2), 515-527. DOI: https://doi.org/10.1016/j.soilbio.2007.09.019

Bašić, F. (2013) The Soils of Croatia. World Soils Book Series. Dordrecht: Springer. DOI: https://doi.org/10.1007/978-94-007-5815-5_1

Baumann, K., Schöning, I., Schrumpf, M., Ellerbrock, R. H., Leinweber, P. (2016) Rapid assessment of soil organic matter: Soil color analysis and Fourier transform infrared spectroscopy. Geoderma, 278, 49-57. DOI: http://dx.doi.org/10.1016/j.geoderma.2016.05.012

Bot, A., Benites, J. (2005) The importance of soil organic matter: Key to drought-resistant soil and sustained food and production. Food and Agriculture Organization of the United Nations.

Bruckman, V. J., Wriessnig, K. (2013) Improved soil carbonate determination by FT-IR and X-ray analysis. Environmental Chemistry Letters, 11, 65–70. DOI: https://doi.org/10.1007/s10311-012-0380-4

Cooperband, L. (2002) Building soil organic matter with organic amendments: A resource for urban and rural gardeners, small farmers, turfgrass managers, and large–scale producers. Center for Integrated Agricultural Systems, University of Wisconsin-Madison.

Demyan, M. S., Rasche, F., Schulz, E., Breulmann, M., Müller, T., Cadisch, G. (2012) Use of specific peaks obtained by diffuse reflectance Fourier transform mid-infrared spectroscopy to study the composition of organic matter in a Haplic Chernozem. Soil Use and Management, 28 (1), 111-119. DOI: https://doi.org/10.1111/j.1365-2389.2011.01420.x

Dhillon, G. S., Gillespie, A., Peak, D., Van Rees, K. C. J. (2017) Spectroscopic investigation of soil organic matter composition for shelterbelt agroforestry systems. Geoderma, 298, 1-13. DOI: https://doi.org/10.1016/j.geoderma.2017.03.016

Fakhry, A., Osman, O., Ezzat, H., Ibrahim, M. (2016) Spectroscopic analyses of soil samples outside Nile Delta of Egypt. Spectrochimica Acta Part A: Molecular and Biomolecular Spectroscopy, 168, 244-252. DOI: https://doi.org/10.1016/j.saa.2016.05.026

FAO (2015) IUSS Working Group WRB - World Reference Base for Soil Resources 2014 update 2015. International soil classification system for naming soils and creating legends for soil maps. World Soil Resources Reports No. 106, Food and Agriculture Organisation of the UN. Available at: https://www.fao.org/3/i3794en/I3794en.pdf [Accessed 3 June 2025].

Ghebleh Goydaragh, M., Taghizadeh-Mehrjardi, R., Golchin, A., Jafarzadeh, A. A., Lado, M. (2021a) Predicting weathering indices in soils using FTIR spectra and random forest models. Catena. DOI: https://doi.org/10.1016/j.catena.2021.105437

Ghebleh Goydaragh, M., Taghizadeh-Mehrjardi, R., Jafarzadeh, A. A., Triantafilis, J., Lado, M. (2021b) Using environmental variables and Fourier Transform Infrared Spectroscopy to predict soil organic carbon. Catena, 202, 105280. DOI: https://doi.org/10.1016/j.catena.2021.105280

Haynes, R. J. (2005) Significance of labile Organic Matter fractions. Advances in Agronomy, Elsevier, 85 (VII), pp. 222-257.

Helfenstein, A., Baumann, P., Viscarra Rossel, R., Gubler, A., Oechslin, S., Six, J. (2021) Quantifying soil carbon in temperate peatlands using a mid–IR soil spectral library, Soil, 7, 193-215. DOI: https://doi.org/10.5194/soil-7-193-2021

Huang, J., Rinnan, Å., Bruun, S., Bruun, T. B., Li, X., Liu, F. (2024) Rapid determination of soil organic carbon and permanganate oxidizable carbon: Comparison of individual and data fusion performance using Fourier transform mid-infrared photoacoustic spectroscopy (FTIR-PAS) and laser-induced breakdown spectroscopy (LIBS). Analytical Letters, 1–18. DOI: https://doi.org/10.1080/00032719.2024.2382270

Hutengs, C., Seidel, M., Oertel, F., Ludwig, B., Vohland, M. (2019) In situ and laboratory soil spectroscopy with portable visible-to-near-infrared and mid-infrared instruments for the assessment of organic carbon in soils. Geoderma, 355, 113900. DOI: https://doi.org/10.1016/j.geoderma.2019.113900

ISO 10390:2005. Soil quality – Determination of pH. International Organization for Standardization.

ISO 11277:2009. Soil quality — Determination of particle size distribution in mineral soil material by sieving and sedimentation. International Organization for Standardization.

ISO 11464:2006. Soil quality – Pretreatment of samples for physico-chemical analysis. International Organization for Standardization.

ISO 13878:2004. Soil quality – Determination of total nitrogen content by dry combustion "elemental analysis". International Organization for Standardization.

ISO 14235:2004. Soil quality – Determination of organic carbon by sulfochromic oxidation (modified; titrimetric determination, Tjurin method, bichromate method). International Organization for Standardization.

Jackson Soil and Root Ecology Lab. (2023) FTIR indicators of soil organic matter quality across a landscape of organic management. University of California, Division of Agriculture and Natural Resources. Available at: https://ucanr.edu/sites/Jackson_Lab/Nitrogen_Cycling_in_Organic_Vegetable_Production/Application_of_FTIR_Spectroscopy_for_SOM_Characterization [Accessed 03 June 2025].

Jadhav, K. P., Ahmed, N., Purakayastha, T. J., Golui, D., Das, R., Meena, M. C., Shrivastava, M., Ranjan, R., Tamuk, P. (2024) Role of clay-humus complexes in soil organic carbon stabilization across paddy soils in diverse Indian soil orders. International Journal of Plant & Soil Science, 36 (11), 527–544. DOI: https://doi.org/10.9734/ijpss/2024/v36i115168

Jensen, J. L., Schjønning, P., Watts, C. W., Christensen, B. T., Obour, P. B., Munkholm, L. J. (2020) Soil degradation and recovery - Changes in organic matter fractions and structural stability, Geoderma, 364, 114181. DOI: https://doi.org/10.1016/j.geoderma.2020.114181

Jiménez-González, M. A., Álvarez, A. M., Carral, P., Almendros, G. (2019) Chemometric assessment of soil organic matter storage and quality from humic acid infrared spectra. Science of The Total Environment, 685, 1160-1168. DOI: https://doi.org/10.1016/j.scitotenv.2019.06.231

Krivoshein, P. K., Volkov, D. S., Rogova, O. B., Proskurnin, M. A. (2022) FTIR Photoacoustic and ATR Spectroscopies of Soils with Aggregate Size Fractionation by Dry Sieving, ACS Omega, 7 (2), 2177-2197. DOI: https://doi.org/10.1021/acsomega.1c05702

Lal, R., Negassa, W., Lorenz, K. (2015) Carbon sequestration in soil. Current Opinion in Environmental Sustainability, 15, 79-86. DOI: https://doi.org/10.1016/j.cosust.2015.09.002

Lehman, R. M., Cambardella, C. A., Stott, D. E., Acosta–Martinez, V., Manter, D. K., Buyer, J. S., Karlen, D. L. (2015) Understanding and Enhancing Soil Biological Health: The Solution For Reversing Soil Degradation. Sustainability, 1 (7), 988-1027. DOI: https://doi.org/10.3390/su7010988

Lei, W., Pan, Q., Teng, P., Yu, J., Li, N. (2023) How does soil organic matter stabilize with soil and environmental variables along a black soil belt in Northeast China? An explanation using FTIR spectroscopy data. CATENA, 228, 107152. DOI: https://doi.org/10.1016/j.catena.2023.107152

Margenot, A. J., Calderón, F. J., Goyne, K., Mukome, F., Parikh, S. J. (2017) Soil analysis, applications of IR and Raman spectroscopies. In: Encyclopedia of Spectroscopy and Spectrometry, 3rd Edition. Oxford Academic Press, 2, 448-454.

Margenot, A. J., Parikh, S. J., Calderón, F. J. (2023) Fourier-transform infrared spectroscopy for soil organic matter analysis. Soil Science Society of America Journal, 87 (5), 1173-1183. DOI: https://doi.org/10.1002/saj2.20583

Maynard, J. J., Johnson, M. G. (2018) Applying fingerprint FTIR spectroscopy and chemometrics to assess soil ecosystem disturbance and recovery, Journal of Soil and Water Conservation, 73 (4), 443-451. DOI: https://doi.org/10.2489/jswc.73.4.443

Metzger, K., Zhang, C., Ward, M., Daly, K. (2020) Mid–infrared spectroscopy as an alternative to laboratory extraction for the determination of lime requirement in tillage soils, Geoderma, 364, 114171. DOI: https://doi.org/10.1016/j.geoderma.2020.114171

Nath, D., Laik, R., Meena, V. S., Kumari, V., Singh, S. K., Pramanick, B., Sattar, A. (2022) Strategies to admittance soil quality using mid-infrared (mid-IR) spectroscopy an alternate tool for conventional lab analysis: A global perspective, Environmental Challenges, 7, 100469. DOI: https://doi.org/10.1016/j.envc.2022.100469

Nocita, M., Stevens, A., van Wesemael, B., Aitkenhead, M., Bachmann, M., Barthès, B., Ben Dor, E., Brown, D. J., Clairotte, M., Csorba, A., Dardenne, P., Demattê, J. A. M., Genot, V., Guerrero, C., Knadel, M., Montanarella, L., Noon, C., Ramirez-Lopez, L., Robertson, J., Sakai, H., Soriano-Disla, J. M., Shepherd, K. D., Stenberg, B., Towett, E. K., Vargas, R., Wetterlind, J. (2015) Soil spectroscopy: An alternative to wet chemistry for soil monitoring. In: D. L. Sparks, ed. Advances in agronomy. Academic Press, Vol. 132, pp. 139-159. DOI: https://doi.org/10.1016/bs.agron.2015.02.002

Nuzzo, A., Buurman, P., Cozzolino, V., Spaccini, R., Piccolo, A. (2020) Infrared spectra of soil organic matter under a primary vegetation sequence, Chemical and Biological Technologies in Agriculture, 7 (6). DOI: https://doi.org/10.1186/s40538-019-0172-1

Obeng, A. S., Dunne, J., Giltrap, M., Tian, F. (2023) Soil organic matter carbon chemistry signatures, hydrophobicity, and humification index following land use change in temperate peat soils. Heliyon, 9, e19347. DOI: https://doi.org/10.1016/j.heliyon.2023.e19347

Padilla, J. E., Calderón, F. J., Acosta-Martinez, V., Van Pelt, S., Gardner, T., Baddock, M., Zobeck, T. M., Noveron, J. C. (2014) Diffuse-reflectance mid-infrared spectroscopy reveals chemical differences in soil organic matter carried in different size wind eroded sediments. Aeolian Research, 14, 99-108. DOI: http://dx.doi.org/10.1016/j.aeolia.2014.06.003

Pärnpuu, S., Astover, A., Tõnutare, T., Penu, P., Kauer, K. (2022) Soil organic matter qualification with FTIR spectroscopy under different soil types in Estonia, Geoderma Regional, 28, e00483. DOI: https://doi.org/10.1016/j.geodrs.2022.e00483

Parolo, M. E., Savini, M. C., Loewy, R. M. (2017) Characterization of soil organic matter by FT-IR spectroscopy and its relationship with chlorpyrifos sorption, Journal of Environmental Management, 196, 316-322. DOI: https://doi.org/10.1016/j.jenvman.2017.03.018

Peltre, C., Bruun, S., Du, C., Thomsen, I. K., Jensen, L. S. (2014) Assessing soil constituents and labile soil organic carbon by mid-infrared photoacoustic spectroscopy. Soil Biology and Biochemistry, 77, 41-50. DOI: https://doi.org/10.1016/j.soilbio.2014.06.022

Rial, M., Martínez Cortizas, A., Rodríguez-Lado, L. (2015) Mapping soil organic carbon content using spectroscopic and environmental data: A case study in acidic soils from NW Spain. Science of the Total Environment, 539, 26-35. DOI: https://doi.org/10.1016/j.scitotenv.2015.08.088

Sanderman, J., Savage, K., Dangal, S. R. S. (2020) Mid-infrared spectroscopy for prediction of soil health indicators in the United States. Soil Science Society of America Journal, 84 (1), 251–261. DOI: https://doi.org/10.1002/saj2.20009

Santos, U. J., Demattê, J. A. M., Menezes, R. S. C., Dotto, A. C., Barbosa Guimarães, C. C., Rodrigues Alves, B. J. R., Sá Barretto Sampaio, E. V. S. (2020) Predicting carbon and nitrogen by visible near-infrared (Vis-NIR) and mid-infrared (MIR) spectroscopy in soils of Northeast Brazil. Geoderma Regional, 23, e00333. DOI: https://doi.org/10.1016/j.geodrs.2020.e00333.

Seidel, M., Hutengs, C., Ludwig, B., Thiele-Bruhn, S., Vohland, M. (2019) Strategies for the efficient estimation of soil organic carbon at the field scale with vis-NIR spectroscopy: Spectral libraries and spiking vs. local calibrations. Geoderma, 354, 113856. DOI: https://doi.org/10.1016/j.geoderma.2019.07.014

Seybold, C. A., Ferguson, R., Wysocki, D., Bailey, S., Anderson, J., Nester, B., Schoeneberger, P., Wills, S., Libohova, Z., Hoover, D., Thomas, P. (2019) Application of mid-infrared spectroscopy in soil survey. Soil Science Society of America Journal, 83, 1746–1759. DOI: https://doi.org/10.2136/sssaj2019.06.0205

Škorić, A. (1982) Priručnik za pedološka istraživanja (engl. Handbook for pedological research). Zagreb: Fakultet poljoprivrednih znanosti.

Socrates, G. (2001) Infrared and Raman characteristic group frequencies: Tables and charts (3rd ed.). John Wiley & Sons, Ltd.

Song, G., Simpson, A. J., Hayes, M. H. B. (2023) Compositional changes in the humin fraction resulting from the long-term cultivation of an Irish grassland soil: Evidence from FTIR and multi-NMR spectroscopies. Science of The Total Environment, 880, 163280. DOI: https://doi.org/10.1016/j.scitotenv.2023.163280

Soriano-Disla, J. M., Janik, L. J., Viscarra Rossel, R. A., Macdonald, L. M., McLaughlin, M. J. (2013) The performance of visible, near-, and mid-infrared reflectance spectroscopy for prediction of soil physical, chemical, and biological properties. Applied Spectroscopy Reviews, 49 (2), 139–186. DOI: https://doi.org/10.1080/05704928.2013.811081

Šoštarić, M., Zgorelec, Ž., Babić, D., Šestak, I., Kisić, I., Mesić, M., Perčin, A. (2017) Radioactivity of Selected Agricultural Soils in Croatia: Effects of Soil Properties, Soil Management, and Geological Parameters. Water Air Soil Pollution, 228, 218. DOI: https://doi.org/10.1007/s11270-017-3398-1

Stenberg, B., Rossel, R. V. (2010) Diffuse reflectance spectroscopy for high-resolution soil sensing. In R. Viscarra Rossel, A. McBratney, B. Minasny, eds. Proximal soil sensing. Springer. DOI: https://doi.org/10.1007/978-90-481-8859-8_3

Sweta, Kumari, S., Dharumarajan, S., Kalaiselvi, B., Gomez, C., Lalitha, M., Das, B., Kusuma, C., Ramakrishnappa, V. (2024) Reviewing the trajectory of Vis-NIR and MIR spectroscopic soil studies in India. Journal of the Indian Society of Soil Science, 23, 23–34. DOI: https://doi.org/10.5958/0974-0228.2024.00026.3

Teong, I. T., Felix, N. L. L., Mohd, S., Sulaeman, A. (2016) Characterization of Soil Organic Matter in Peat Soil with Different Humification Levels using FTIR, IOP Conference Series: Materials Science and Engineering, 136, 1, 012010. DOI: https://doi.org/10.1088/1757-899X/136/1/012010

Thabit, F. N., Negim, O. I. A., AbdelRahman, M. A. E., Scopa, A., Moursy, A. R. A. (2024) Using Various Models for Predicting Soil Organic Carbon Based on DRIFT-FTIR and Chemical Analysis. Soil Systems, 8 (1), 22. DOI: https://doi.org/10.3390/soilsystems8010022

Tinti, A., Tugnoli, V., Bonora, S., Francioso, O. (2015) Recent applications of vibrational mid-infrared (IR) spectroscopy for studying soil components: A review. Journal of Central European Agriculture, 16 (1), 1-22. DOI: https://doi.org/10.5513/JCEA01/16.1.1535

Vohland, M., Ludwig, M., Thiele-Bruhn, S., Ludwig, B. (2014) Determination of soil properties with visible to near- and mid-infrared spectroscopy: Effects of spectral variable selection. Geoderma, 223–225, 88–96. DOI: https://doi.org/10.1016/j.geoderma.2014.01.013

Volkov, D. S., Rogova, O. B., Proskurnin, M. A. (2021) Organic Matter and Mineral Composition of Silicate Soils: FTIR Comparison Study by Photoacoustic, Diffuse Reflectance, and Attenuated Total Reflection Modalities, Agronomy, 11, 1879. DOI: https://doi.org/10.3390/agronomy11091879

Wang, J., Zhen, J., Hu, W., Chen, S., Lizaga, I., Zeraatpisheh, M., Yang, X. (2023) Remote sensing of soil degradation: Progress and perspective, International Soil and Water Conservation Research, 11, 429-454. DOI: https://doi.org/10.1016/j.iswcr.2023.03.002

Wasner, D., Abramoff, R., Griepentrog, M., Venegas, E. Z., Boeckx, P., Doetterl, S. (2024) The role of climate, mineralogy, and stable aggregates for soil organic carbon dynamics along a geoclimatic gradient. Global Biogeochemical Cycles, 38, e2023GB007934. DOI: https://doi.org/10.1029/2023GB007934

Wijewardane, N. K., Ge, Y., Sanderman, J., Ferguson, R. (2021). Fine grinding is needed to maintain the high accuracy of MIR spectroscopy for soil property estimation. Soil Science Society of America Journal, 85, 263–272. DOI: https://doi.org/10.1002/saj2.20194

Wijewardane, N. K., Ge, Y., Wills, S., Libohova, Z. (2018) Predicting physical and chemical properties of US soils with a mid-infrared reflectance spectral library. Soil Science Society of America Journal, 82 (3), 722–731. DOI: https://doi.org/10.2136/sssaj2017.10.0361

Williams, M. I., Farr, C. L., Page–Dumroese, D. S., Connolly, S. J. (2020) Soil Management and Restoration. In: Forest and Rangeland Soils of the United States Under Changing Conditions.

Xing, Z., Du, C., Shen, Y., Ma, F., Zhou, J. (2021) A method combining FTIR-ATR and Raman spectroscopy to determine soil organic matter: Improvement of prediction accuracy using competitive adaptive reweighted sampling (CARS). Computers and Electronics in Agriculture, 191, 106549.
DOI: https://doi.org/10.1016/j.compag.2021.106549

Xu, X., Du, C., Ma, F., Shen, Y., Zhou, J. (2020) Forensic soil analysis using laser-induced breakdown spectroscopy (LIBS) and Fourier transform infrared total attenuated reflectance spectroscopy (FTIR-ATR): Principles and case studies. Forensic Science International. DOI: http://dx.doi.org/10.1016/j.forsciint.2020.110222

Ye, C., Zhu, T., Guo, H., Li, J., Nie, M. (2024) Comparison of infrared and solid-state 13C NMR spectroscopy for assessing soil organic carbon composition following hydrofluoric acid treatment. Fundamental Research, In press.
DOI: https://doi.org/10.1016/j.fmre.2024.12.011

Zebec, V., Rastija, D., Lončarić, Z., Bensa, A., Popović, B., Ivezić, V. (2017) Comparison of Chemical Extraction Methods for Determination of Soil Potassium in Different Soil Types, Eurasian Soil Science, 50 (12), 1420-1427. DOI: https://doi.org/10.1134/S1064229317130051

Zimmermann, M., Leifeld, J., Fuhrer, J. (2007) Quantifying soil organic carbon fractions by infrared spectroscopy. Soil Biology and Biochemistry, 39 (1), 224–231.
DOI: https://doi.org/10.1016/j.soilbio.2006.07.010

APPENDICES

Table 1. IR absorption band positions with the assignation of the underlying molecular vibrations according to the scientific literature.

Band position (cm^{-1})	Functional group assignment and type of vibration	Associated soil constituents (literature data*)
3700 – 3200	O–H, N–H stretching	clay minerals, amides [21]
3698	Si–OH, Fe–O stretching	clay minerals (kaolinite, gibbsite) [1]
3696	Si–OH stretching	clay minerals (kaolinite, montmorillonite) [11]
3697 – 3689	O–H stretching	kaolinite [15]
3694	O–H stretching	clay minerals [2,22], quartz [2]
3692	O–H stretching	clay minerals [13]
3690 – 3680	Si–OH, O-H stretching	clay minerals [10]
3630	O–H stretching	clay minerals [21]
3629 – 3618	O–H stretching	kaolinite [3]
3627	O–H stretching	clay minerals [13]
3622	Si–OH, Fe–O stretching	clay minerals (kaolinite, gibbsite) [1]
3620	(Al)/(Mg)Si–OH, O–H stretching	clay minerals (kaolinite, montmorillonite) [4,10,11,18,19]
3620 – 3613	(Al)–OH stretching	smectite [15]
3617	O–H stretching	clay minerals, quartz [2]
3600 – 3000	O–H stretching	alcohols, phenols, water [17]
3600 – 2800	O–H, N–H stretching	alcohols, phenols, amides, water [19]
3553 – 3542	O–H stretching	phenols [15]
3500 – 3300	O–H, N–H stretching	alcohols, phenols, carboxylic acids, amides [20]
3500 – 3200	O–H, N–H stretching	alcohols, phenols, amine, amide,carboxyl and hydroxyl groups [18]
3490	O–H stretching	alcohols, phenolics, carboxylic acids [4,10]
3460	O–H stretching	clay minerals (gibbsite) [1]
3450	O–H stretching	clay minerals, water [8]
3450 – 3420	O–H stretching	clay minerals [15]

Continued. Table 1

Band position (cm^{-1})	Functional group assignment and type of vibration	Associated soil constituents (literature data*)
3440 – 3320	O–H, N–H stretching	clay minerals, amines [1]
3430	O–H stretching	water [1]
3430 – 3401	O–H stretching	water, carboxyl and hydroxyl groups of SOM [3]
3394	O–H stretching	cellulose [22]
3365	O–H, N–H stretching	alcohols, phenols, carboxyls, amides and amines [2]
3360	O–H stretching	clay minerals [11]
3351	O–H stretching	alcohols [5]
3340	O–H stretching	cellulose [6]
3270	O–H, C=O stretching	alcohols, phenolics, carboxylic acids [4,10]
3107 – 3042	Aryl-H, C=C stretching	aromatics [1]
3000 – 2800	C–H stretching	aliphatics [1,19]
2983	C–H asymmetric stretching	aliphatics [12]
2960	C–H stretching	aliphatics [20]
2947 – 2858	C–H stretching	aliphatics [3]
2940	C–H asymmetric stretching	aliphatics [4]
2930 – 2910	C–H asymmetric stretching	aliphatics [10]
2930 – 2870	C–H stretching	aliphatics [21]
2930	C–H asymmetric stretching	aliphatics [1,7]
2929 – 2917	C–H symmetric stretching	humic acids, fulvic acids, humic [15]
2925	C–H stretching	aliphatics [16]
2921	C–H asymmetric stretching	aliphatics [2,12]
2920	C–H asymmetric stretching	aliphatics (fats, wax, lipids) [5,6,8,13,17]
2910	C–H asymmetric stretching	aliphatics [9]
2879	C–H stretching	aliphatics [20]

Continued. Table 1

Band position (cm^{-1})	Functional group assignment and type of vibration	Associated soil constituents (literature data*)
2860 – 2850	C–H symmetric stretching	aliphatics (fats, wax, lipids) [10]
2860	C–H symmetric stretching	aliphatics [4]
2858	C–H stretching	aliphatics [16]
2856 – 2849	C–H asymmetric stretching	humic acids, fulvic acids, humic [15]
2855	C–H symmetric stretching	aliphatics (fats, wax, lipids) [7]
2852	C–H symmetric stretching	aliphatics [2]
2850	C–H symmetric stretching	aliphatics (fats, wax, lipids) [5,6,8,13,17], polysaccharides [5,6,8]
2627	C–H stretching	carbonates (aragonite) [1]
2592	C–H stretching	carbonates (calcite) [1]
2520	C–H stretching	carbonates (calcite, aragonite) [1, 19]
2514 – 2507	C–O vibration	carbonates (calcite, dolomite) [3]
2500	O–H stretching	carbonates [7]
2500 – 2400	O–H stretching	carbonates [13]
2200 – 2000	C–OH vibration	carbohydrates [19]
2137	C–OH vibration	carbohydrates [22]
2000	Si–O stretching	quartz [1]
2000 – 1790	Si–O stretching	quartz [19,21]
1993	Si–O stretching	silicates [22]
1900 – 1700	C=O stretching	humic acids [15]
1885	C=O stretching	carboxylic acids [10]
1880 – 1866	Si–O, C=O stretching	quartz, clay minerals, carboxylic acids [4]
1870	Si–O stretching	silicates [22]
1865	C=O stretching	carboxylic acids [10]
1800	C=O stretching	carbonates (calcite) [1]

Continued. Table 1

Band position (cm^{-1})	Functional group assignment and type of vibration	Associated soil constituents (literature data*)
1790 – 1783	C=O stretching	carbonates (calcite) [10]
1788	Si–O stretching	silicates [22]
1783	Si–O, C=O stretching	clay and quartz minerals, carboxylic acids [4]
1730 – 1700	C=O stretching	carboxylic acids, humic acids [1,8]
1730 – 1720	C=O stretching	carboxylic acids [10]
1720 – 1710	C=O stretching	carboxylic acids [19]
1720 – 1700	C=O stretching	carboxylic acids [20]
1720	C=O stretching	carboxylic acids [6, 14], aromatic esters [6]
1713	C=O stretching	aromatics [12]
1710 – 1707	C=O stretching	free organic acids [6]
1710 – 1680	C=C stretching, N–H bending	amines, alkenes (aromatics) [10]
1703	C=C, C=O stretching	carboxylic acids, esters [17]
1702	C=O stretching	carboxylic acids [5]
1670 – 1600	C=C, C=O stretching	amide II, phenyls, carboxyls [21]
1660 – 1640	C=O stretching	amides [19]
1660 – 1600	C=O stretching	aromatics [19]
1656	C=O stretching	amides [22]
1653	C=O stretching	aromatics, amides, amide I [6]
1650 – 1600	C=C, C=O stretching	aromatics, aliphatics, lignin, carboxylates [6,20]
1650 – 1640	O–H, C=C stretching	aromatics, amide I, primary water [4,10]
1650	C=O, C–N stretching	amide I, ketones, carboxyls, quinones, lignins [1], aromatics [9]
1647 – 1633	N–H bending	primary and secondary amides [3]
1644	C=O stretching	aromatics, amides, ketones, lignin, humic acids [17]
1643 – 1615	C=O stretching	carboxylates [15]

Continued. Table 1

Band position (cm^{-1})	Functional group assignment and type of vibration	Associated soil constituents (literature data*)
1642 – 1569	C=C, C=O stretching	amide II, aromatics, quinones, carboxylates [1]
1640 – 1620	C=O stretching	amides [12]
1640	C=O stretching	aromatics, quinones, amides [14]
1634	C=O stretching	aromatics [16]
1633	C=C, C=O stretching, C–N stretching	aromatics, amide I [2]
1630	C=C, C=O, O–H stretching	aromatics, amides [18], clay minerals [11], water [19]
1620 – 1610	Si–O, C=O stretching, N–H bending	silicates, aromatics, amide I [4,10]
1620	C=O stretching	aromatics [14]
1616	C=O stretching	aromatics, amides [22]
1610	C=O, C=C stretching	aromatics, ketones [12], amines [19]
1606	C=O stretching	aromatic amines [5]
1600 – 1598	C=C stretching	aromatics [10]
1600 – 1570	C=C stretching	aromatics, carboxylates [19]
1584	C=O, C=C stretching	aromatic phenols lignin, humic acids [17]
1580	C=C, C=O asymmetric stretching	aromatics [10]
1580 – 1551	C=C, C=O asymmetric stretching	aromatics, alkenes [8]
1570 – 1540	N–H and C–N in-plane bending	amide II [19]
1564	C=O stretching	amide II [16]
1560 – 1480	N–H and C–N in-plane bending, C–H, C=C, C=N stretching	amide II , aromatics [21]
1550	N–H in-plane bending, C=C stretching	amide II 6, aromatics [11]
1540 – 1520	Si–O, C=C stretching	quartz, amide II, aromatics [10,14]
1540	Si–O, C=C, C=O stretching	silicates, aromatics [13], amides [14]
1530 – 1510	C=C stretching	aromatics, amide II, phenols, lignin [1]
1521	C=C stretching	Lignin [22]

Continued. Table 1

Band position (cm^{-1})	Functional group assignment and type of vibration	Associated soil constituents (literature data*)
1520	C=C stretching	aromatics, amides (amide II) [12,13]
1515	C=C stretching	aromatics, amide II [8,19]
1515 – 1513	C=C stretching	phenolics, lignin [6]
1510	C=C stretching	lignin [14]
1509	C–H, C=C stretching	aromatics [17]
1508	C=C stretching	lignin [5,6]
1490	C=C stretching	aromatics 9
1479 – 1444	C–H, N–H stretching	amide II, aliphatics [1]
1465	C–H stretching	aliphatics [4,7,9,19], organo-clay complexes [19]
1460	Si–O stretching, O–H, C–H scissoring	silicates [4], amides [10] lignin [14]
1453 – 1416	C–O stretching, C–H bending	calcite, dolomite, aromatics, phenolics [3]
1450 – 1370	C–H bending	aromatics [20]
1450	C–H bending	aliphatics [6,7], phenolics, lignin [6]
1445 – 1350	C–H bending	methyls [19]
1440	C–O–H in-plane bending	carboxyls [10], carbonates [11,18,20]
1435 – 1419	C–O stretching	calcite [15]
1430	C–O stretching	carbonates [17,19]
1434	C–H bending	aliphatics [17]
1426	C–O, C=C, O–H stretching	carboxylic acids (humic acids) [6,10], aromatics, aliphatics
1423	C–O stretching	carboxylates [22]
1420	(Mg)–OH, C–O stretching	clay minerals, carboxyls [10], lignin [14], carboxylates, aromatics, amides [16]
1417	C–H, C–OH bending, C–O, C=O stretching	aliphatics, carbonates [2]
1415	C–O stretching, C–H bending	phenolics, carboxylic acids (benzoic acid) [1]
1410	C–O, O–H stretching	phenolics [12]

Continued. Table 1

Band position (cm^{-1})	Functional group assignment and type of vibration	Associated soil constituents (literature data*)
1410 – 1400	(Mg)–OH, C–O stretching	quartz, carboxylic acids [4]
1400	C–H symmetric stretching	carboxylic acids [8]
1400 – 1300	O–H stretching	montmorillonite, nontronite [13]
1397 – 1384	C–O stretching	carboxylates [15]
1396 – 1383	C–O stretching	calcite, dolomite, aromatics, phenolics [3]
1393	C–O stretching	carboxylates [19]
1380	C–H, C–O, O–H bending	phenolics, carboxyls [1]
1373	O–H stretching	montmorillonite, nontronite [13]
1371	C–H bending	phenolics, lignin, aliphatics [6]
1370	C–H, C–O stretching	aliphatics, lignin-derived phenols [17]
1342 – 1307	C–N stretching	aromatic amines [1]
1320	O–H deformation	carbonates [7]
1320 – 1310	C–H, C–O stretching	amide III, aromatics, carboxylic acids [10]
1320 – 1230	C–N stretching	amide III [19]
1320 – 1220	O–H, C–H bending, C–O stretching	amide III, carboxylic acids, esters, phenols [21]
1295 – 1220	C–OH, C–H bending	phenols, aromatics [19]
1293 – 1256	C–O stretching	bentonite, benzoic acid, ethers [1]
1285 – 1280	Si–O, C–O, C–N stretching, C–H rocking	clay minerals, aromatics, carboxylic acids [10]
1280 – 1200	C–O stretching	carboxylic acids, phenols, esters [21]
1270	C–O stretching	aliphatics 8, lignin [14]
1265	C–O stretching	phenolics, ethers, lignin [6]
1250 – 1050	Si–O stretching	quartz [21]
1240	C–O stretching	phenolics [9]
1238	Si–O stretching	silicates [1]

Continued. Table 1

Band position (cm^{-1})	Functional group assignment and type of vibration	Associated soil constituents (literature data*)
1235 – 1225	C–O stretching	carboxylic acids [8]
1230	C–O stretching, O–H deformation	carboxyls, phenols, aryl ethers, acetates [1], lignin [14]
1170 – 1060	C–O stretching	polysaccharides, proteins [19]
1170 – 1000	C–O stretching	carbohydrates, proteins, nucleic acids [21]
1165	Si–O stretching	quartz [4]
1165 – 1153	Si–O, O–H, C–O–H stretching	quartz, aliphatics [10]
1162	C–O stretching	polysaccharides [17]
1160	C–OH stretching	aliphatics, alcohols, carbohydrates [1]
1160 – 1030	Si–O, C–OH stretching	clay minerals, quartz, cellulose [17]
1159	C–O stretching	polysaccharides, proteins, nucleic acids [22]
1136 – 1070	Si–O, SiO–H, C–OH stretching	silicates, sulfates, alcohols, alkyl ethers [1]
1130	C–H bending	lignin [14]
1115 – 1105	Si–O, C–O stretching	silica, carboxyls [10]
1113	Si–O stretching	silicates [4]
1110	C–OH stretching	alcohols [12]
1107 – 914	Si–O stretching	silicates [15]
1103	C–O stretching	polysaccharides [17]
1100 – 1000	Si–O stretching	silicates (quartz) [13,19]
1095	Si–O, C–H in-plane bending	silicates, non-aromatics [4,10]
1085	Si–O, C–H in-plane bending	minerals, polysaccharides [16]
1080 – 1075	Si–O stretching, C–N stretching	clay minerals (kaolinite, illite), polysaccharides [10]
1080 – 1030	C–O, O–H stretching	polysaccharides [6]
1070	Si–O stretching	silicates (kaolinite, illite) [4,8]
1066	Si–O stretching	montmorillonite, nontronite [13]

Continued. Table 1

Band position (cm^{-1})	Functional group assignment and type of vibration	Associated soil constituents (literature data*)
1060	O–H stretching	polysaccharides [22]
1056 – 945	SiO–H, C–O stretching, C=C bending	aluminosilicates (kaolinite, illite, smectite), carbohydrates (polysaccharides), sulfones, aromatics [1]
1050	C–O, O–H stretching	polysaccharides [12,19,20,21]
1046 – 1025	Si–O stretching	kaolinite [3]
1039 – 1024	Si–O stretching	montmorillonite [15]
1037	(Al)–OH, Si–O stretching, C–H in-plane bending	clay minerals (kaolinite, illite) [10], polysaccharides [10,17]
1035 – 1020	Si–O stretching, C–H bending	silicates (kaolinite, illite), non-aromatics [4]
1033	Si–O, C–H in-plane bending	silicates, polysaccharides [16]
1030	Si–O, C–H bending	silicates [13], lignin [14]
1030 – 950	Si–O stretching	clay minerals [19]
1010 – 995	Si–O stretching	kaolinite, illite [10]
1002	Si–O, C–O stretching	clay minerals, polysaccharides [2]
1000	Si–O lattice stretching	silicates (kaolinite, illite) [4,18,22]
990	(Al)–OH deformation	aluminosilicates, clay minerals [11]
975	Si–O, C–O, C=C stretching, C–H out-of-plane bending	aluminosilicates (kaolinite, illite, smectite) [10], sulfones, aromatics [1]
975 – 675	C–H out-of-plane bending	aromatics [19]
945 – 887	C=C stretching	benzoic acid, carbohydrates, cellulose [1]
930 – 910	Si–O stretching, C–O–H out-of-plane bending	aluminosilicates, benzoic acid, carbohydrates, cellulose [4,10]
926 – 912	(Al)–OH stretching	aluminosilicates [15]
925	(Al)–OH stretching	kaolinite [18]
920	(Al)–OH stretching	aluminosilicates (kaolinite) [1]
916	O–H stretching	kaolinite, smectite [22]
915	(Al)–OH stretching	kaolinite, smectite [19]
910 – 900	C–H out-of-plane bending	aromatics [8]

Continued. Table 1

Band position (cm^{-1})	Functional group assignment and type of vibration	Associated soil constituents (literature data*)
910	(Al)–OH stretching	aluminosilicates, clay minerals [11]
900	O–H stretching	cellulose [6]
891 – 870	O–H stretching	calcite [15]
887 – 866	O–H stretching	carbonates, quartz and clay minerals [1]
875	SiO–H stretching, C–H bending	carbonates (calcite) [10,13,19], aromatics [10]
873	SiO–H stretching	carbonates [22]
870	C–H, C=C stretching	aromatics [1]
870 – 800	(Al)/ (Mg)–OH stretching	smectite [13]
860	(Al)–OH stretching	clay minerals [4,10]
850 – 750	N–H out-of-plane bending	primary amines [19]
848	N–H out-of-plane bending	primary amines [22]
835	C–H out-of-plane bending	aromatics, lignin [1,6]
820 – 752	O–H, C–C stretching	kaolinite, carbonates, phenols, cellulose [1]
811	Si–O stretching	quartz [22]
800	Si–O stretching	quartz, silicates [8,13,19]
798 – 779	Si–O stretching	quartz [3]
796	Si–O lattice stretching, C–H out-of-plane bending	silicates, non-aromatics [4,10]
794 – 777	Fe(II)–OH stretching	clay minerals [15]
780	Si–O stretching, N–H out-of-plane bending	quartz, silicates [8,13], primary amines [18]
774	Si–OH, (Al)/ (Mg)–OH stretching	clay minerals [10]
750	Si–OH, (Al)/(Mg)–OH stretching, C–H bending	clay minerals, polyaromatics [10]
750 – 700	N–H wag	secondary amines [19]
720	C–H bending (CH2 wag)	carbonates (calcite) [1], alkanes [1,6]
716 – 713	C–O vibrations	calcite [3]

Continued. Table 1

Band position (cm^{-1})	Functional group assignment and type of vibration	Associated soil constituents (literature data*)
715	O–H, C–H bending	water, alkanes [10]
712	C–O vibrations	calcite [13]
700	Si–O bending	silica [1,19]
700 – 600	Fe–O vibrations	iron oxides [19]
698 – 686	C–H out-of-plane bending	aromatics [3]
697 – 696	Si–O lattice bending	silicates, quartz [4,10]
695	Si–O lattice bending	silicates, quartz [8]
693 – 673	Si–O bending	quartz [15]
698 – 686	C–H out-of-plane bending	aromatics [3]
675 – 670	C–H bending	aromatics [10]
655 – 650	Si–O bending, Fe–O stretching	silicates [1,4,10]
650 – 580	Si–O, Si–O–(Al)/(Mg) bending, Fe–O stretching	clay minerals [13]
645 – 640	Si–O, S–C, O–H stretching	silicates (bentonite), sulfates, water [10]
630 – 620	Ca–OH, C–S stretching	hydroxyapatite, carbonates and sulfates [10]
550 – 445	Si–O, Si–O–(Al) bending	silicates [13]
536 –525	O–H stretching	metal oxides [15]
535 – 525	Si–O–Al bending	kaolonite [10]
520	Si–O–Al bending	silicates [1]
517 – 513	Si–O lattice bending	quartz [10]
500 – 400	Si–O lattice bending	clay minerals (kaolinite, illite, smectite) [13]
490	Si–O lattice bending	silicates, water [4,10]
470	Si–O, Si–O–(Al) bending, Fe–O stretching	silicates [1,4,8,10]
470 – 420	Si–O lattice bending	clay minerals (kaolinite, illite, smectite) [1]
450	Si–O lattice bending	silicates [10]

Continued. Table 1

Band position (cm^{-1})	Functional group assignment and type of vibration	Associated soil constituents (literature data*)
455 – 450	Si–O lattice bending	silicates [4]
440	Si–O lattice bending	silicates [4]
430 – 420	(Al/Mg) –OH stretching, C–C in-phase vibrations	clay minerals (kaolinite, illite, smectite), quartz [4,8]
400	Si–O lattice bending	silicates [4]

[*1] (Tinti et al. (2015);
[2] Pärnpuu et al. (2022);
[3] Parolo et al. (2017);
[4] Krivoshein et al. (2022);
[5] Teong et al., 2016);
[6] Artz et al. (2008);
[7] Helfenstein et al. (2021);
[8] Nuzzo et al. (2020);
[9] Maynard and Johnson (2018);
[10] Volkov et al. (2021);
[11] Xing et al. (2021);
[12] Obeng et al. (2023);
[13] Ghebleh-Goydaragh et al. (2021a);
[14] Jiménez-González et al. (2019);
[15] Fakhry et al. (2016);
[16] Baumann et al., 2016);
[17] Dhillon et al. (2017);
[18] Xu et al. (2020);
[19] Peltre et al. (2014);
[20] Ghebleh-Goydaragh et al. (2021b);
[21] Padilla et al. (2014);
[22] Nath et al. (2022).

Table 2. Sampling parameters in the studied areas of Croatia

Soil type (FAO, WRB, 015)	Coordinates, (GPS - Garmin GPSmap 60C)	Sample location	Region	Land use type	Sampling depth (cm)	Sampling year
Luvisol	N 45°20'40.50" E 13°35'25.30"	Novigrad	Western Croatia (Istra peninsula)	Olive trees – Fire range	0 – 10	2020
Regosol acric	N 46°7' 16.80" E 17° 0' 22.98"	Molve 40	Northern Croatia	Arable cropland	0 – 30	2023
Gleysol vertic	N 46°6' 38.58" E 17°0' 37.62"	Molve 9	Northern Croatia	Meadow	0 – 30	2023
Dystric Stagnosol	N 45°33'20" E 16°31'49"	Potok	Central Croatia	Conventional agriculture	0 – 30	2018
Chernozem	N 450 24' 6.46" E 180 56' 6.59"	Vukovar	Eastern Croatia	Conventional agriculture	0 – 30	2015

Table 3. Physical characteristics of the examined soil types

Soil type (WRB-FAO, 2015)	Particle size distribution (%)			Texture
	Clay	Silt	Sand	
Luvisol	57	40	3	Silty Clay
Regosol acric	7	11	82	Loamy sand
Gleysol vertic	54	39	7	Clay
Dystric Stagnosol	14	30	56	Sandy loam
Chernozem	30	67	3	Silty clay loam

Table 4. Chemical characteristics of the examined soil types including: pH, Organic Matter (OM%), Total Nitrogen (TN %), plant available Phosphorus (P_{AL}) and plant available Potassium (K_{AL})

Soil type (WRB-FAO, 2015)	pH_{KCl}	OM (%)	TN (%)	P_{AL}, (mg/kg soil)	K_{AL}, (mg/kg soil)
Luvisol	6.30	3.4	0.237	41	256
Regosol acric	5.32	2.4	0.118	136	184
Gleysol vertic	4.83	10.9	0.710	30	194
Dystric Stagnosol	4.84	1.3	0.080	106	129
Chernozem	6.80	3.3	0.451	315	431